https://doi.org/10.5194/tc-2019-132
Preprint. Discussion started: 8 July 2019

The Cryosphere Discussions

Multi-modal sensing drifters as a tool for repeatable glacial hydrology flow path measurements

Andreas Alexander[1, 2], Maarja Kruusmaa[3, 4], Jeffrey A. Tuhtan[3], Andrew J. Hodson[2, 5], Thomas V. Schuler[1, 6], and Andreas Kääb[1]

[1]Department of Geosciences, University of Oslo, 0316 Oslo, Norway
[2]Department of Arctic Geology, The University Centre in Svalbard, 9171 Longyearbyen, Norway
[3]Centre for Biorobotics, Tallinn University of Technology, 12618 Tallinn, Estonia
[4]Centre for Autonomous Marine Operations and Systems, Norwegian University of Science and Technology, 7491 Trondheim, Norway
[5]Department of Environmental Sciences, Western Norway University of Applied Sciences, 6856 Sogndal, Norway
[6]Department of Arctic Geophysics, The University Centre in Svalbard, 9171 Longyearbyen, Norway

Correspondence: Andreas Alexander (andreas.alexander@geo.uio.no)

Abstract. Lagrangian drifters are a practical way to measure natural flow features in surface channels. In this study, small cylindrical drifters (length 12 cm, diameter 4 cm) were deployed in a supraglacial channel. Each drifter recorded the total water pressure, linear acceleration, magnetic field strength and rate of rotation at 100 Hz. Based on an ensemble analysis of repeated field deployments (n = 55), it was found that the pressure sensors consistently delivered the most accurate data, where values remained within ±0.11% of the total pressure time-averaged mean (95% confidence interval). Magnetometer readings also exhibited low variability across deployments, maintaining readings within ±2.45% of the time-averaged mean of the magnetometer magnitude. Linear acceleration measurements were found to have substantially larger 95% confidence intervals, spanning ±34.4% from the time-averaged mean magnitudes. Furthermore, the drifter speed along the supraglacial channel was estimated by integrating the linear acceleration, providing a 95% confidence interval of ±24.5% of the time-averaged mean magnitude. The major contribution of this work is to provide a statistical assessment of multimodal drifters, repeatedly deployed in a 450 m long supraglacial channel reach, with a focus on developing a repeatable field measurement methodology including uncertainty. The results of this work show that multimodal drifters are capable of highly repeatable field measurements in supraglacial channels.

1 Introduction

Subglacial hydrology remains an important field of research due to its role in glacier dynamics (Flowers, 2018), sediment evacuation and its impact on fjord and proglacial ecosystems (e.g. Swift et al., 2005; Meire et al., 2017; Urbanski et al., 2017). The limited access to the subglacial environment complicates direct measurements and observations. Earlier works have acknowledged the role of subglacial water in glacier sliding (e.g. Weertman, 1972; Engelhardt and Kamb, 1998). Surface water was found to control the basal motion of glaciers (e.g. Iken, 1972; Iken and Bindschadler, 1986; Hubbard and Nienow, 1997; Anderson et al., 2004; Harper et al., 2010), as well as larger ice caps and ice sheets (e.g. Zwally et al., 2002; Van de Wal

https://doi.org/10.5194/tc-2019-132
Preprint. Discussion started: 8 July 2019

et al., 2008; Benn et al., 2009; Sundal et al., 2011; Stearns and van der Veen, 2018). Surface water is thereby able to enter the subglacial system through moulins, cracks, crevasses and cut-and-closure systems (Gulley et al., 2009). Ice-walled drainage systems have highly variable geometry, controlled by the counteracting mechanisms of melt enlargement due to dissipation of potential energy and creep-closure of the viscous ice (Röthlisberger, 1972). Therefore, the capacity of the glacial drainage system adjusts to variable supply by melt water from the surface (Schoof, 2010; Bartholomew et al., 2012). Step-pool sequences are formed as a series of geometric adjustments (e.g. Vatne and Irvine-Fynn, 2016) and represent up to 90% of the total flow resistance of a stream (Curran and Wohl, 2003), leading to an important role of channel pattern and morphology on flow resistance and water velocity (Germain and Moorman, 2016). Water velocity was also shown to control the incision rates in ice-walled channels in conjunction with water temperature and the rate of heat loss at the channel boundaries (Lock, 1990; Isenko et al., 2005; Jarosch and Gudmundsson, 2012). Despite these advances, major knowledge gaps remain. Largely unknown are the mechanisms behind how water is routed from the glacier surface to the bed. The role of subglacial water on glacier dynamics therefore requires new methods for the direct measurements of the subglacial environment including the water temperature, the velocities as well as the pressures and the flow path morphology along multiple flow paths.

However useful, direct measurements are scarce and difficult to obtain. This is largely due to the limited accessibility of the subglacial environment which is governed by high pressures (Iken and Bindschadler, 1986; Rada and Schoof, 2018), high sedimentation rates (Walder and Fowler, 1994), abrasion (Haldorsen, 1981) and turbulent water flow (Kor et al., 1991). Beginning in the early 2000s, new technologies have emerged (presented in more detail in Table 1), which open new, promising pathways towards an improved understanding of subglacial hydrology (e.g. Martinez et al., 2004; Hart et al., 2006; Rose et al., 2009; Hart et al., 2011a; Smeets et al., 2012; Bagshaw et al., 2012, 2014; Hart et al., 2015; Bagshaw et al., 2018; Hart et al., 2019). Current methods for in-situ tests include dye tracing (e.g. Seaberg et al., 1988; Willis et al., 1990; Fountain, 1993; Nienow et al., 1998; Hasnain et al., 2001; Schuler and Fischer, 2009), salt injection gauging (e.g. Willis et al., 2012) geophysical methods (e.g. Diez et al., 2019), and direct observations are available from borehole instrumentation (e.g. Iken and Bindschadler, 1986; Engelhardt et al., 1990; Hubbard et al., 1995; Stone and Clarke, 1996). There are also encouraging attempts to deploy sensors in moulins (Iken, 1972; Vieli et al., 2004). Direct access of the glacier base has been exploited to collect measurements at the subglacial laboratory in Engabreen, Norway (e.g. Cohen et al., 2006; Iverson et al., 2007) as well as at the Argentière glacier in the French Alps (e.g. Vivian and Bocquet, 1973; Goodman et al., 1979; Hantz and Lliboutry, 1983).

Most of the recent developments in sensors in glacial hydrology (see Table 1 for a detailed overview) have been focused on devices which can perform borehole measurements which can be transferred wirelessly through the ice (e.g. Martinez et al., 2004; Hart et al., 2006; Rose et al., 2009; Smeets et al., 2012; Hart et al., 2019). The major limitations of fixed position observations is that they have to be deployed via borehole, decreasing the chances to enter a subglacial system, and that boring requires a high deployment cost. This has motivated the development of Lagrangian sensors which move with the changing environment, thus providing a wider range of observational data at a substantially lower deployment cost. Drifters are small devices which passively follow the water flow and are commonly used in large-scale surface flow studies and are able to pro-

https://doi.org/10.5194/tc-2019-132
Preprint. Discussion started: 8 July 2019

vide information about their position and speed (Landon et al., 2014). Depending on their sensor payload, drifters can be used for a wide range of applications, including coastal and ocean surface current monitoring (Boydstun et al., 2015; Jaffe et al., 2017), to estimate river bathymetry and surface velocities (Landon et al., 2014; Almeida et al., 2017) and to collect imagery for underwater photogrammetry (Boydstun et al., 2015).

The use of sensing drifters in glaciology has been previously reported, most notably the Moulin Explorer by Behar et al. (2009), which was unfortunately lost during its first deployment, and the development was afterwards discontinued. A successful glacial drifter was the E-tracer, as reported by Bagshaw et al. (2012). The device was the size of a table tennis ball and included a radio transmitter capable of transmitting through the subglacial environment on the margin of Leverett Glacier in Greenland, reemerging at the glacier portal (Bagshaw et al., 2012). These encouraging results lead to a second generation of E-tracers equipped with a pressure sensor, and successfully transmitted pressure data from subglacial channels through 100 meters of overlying ice after having been deployed in crevasses and moulins (Bagshaw et al., 2014). The published data remains however sparse and limited to a single mean pressure plot in Bagshaw et al. (2014). As with all new field measurement technologies, the repeatability of in-situ measurements is often very challenging to determine. Encouraged by the previous drifter studies from Bagshaw et al. (2012) and Bagshaw et al. (2014) with a single pressure sensor, the present study explores the potential of multi-modal sensing drifters to extract data along the flow path of glacier channels. The focus of this work is to assess the repeatability of Lagrangian drifter measurement data, with a specific focus on glacial hydrology. Current methods, such as dye tracing, allow for the repeatable measurement of the flow velocities averaged over the duration of a passage. However, it is impossible to deconvolve these records to obtain spatially and temporally distributed information. The present study assesses the potential of sensing drifters to acquire spatial and temporal variation of the velocity along a flow path. Furthermore, the multi-modal sensor data are investigated for potential time series features that may be associated with geometrical features of the supraglacial channel. The experiments are achieved by using a submersible multi-modal drifter platform measuring at 100 Hz. The small, low-cost (500 EUR) platform records total water pressures, linear acceleration, rotation rates and the magnetic field strength via repeated deployments along a section of supraglacial meltwater channel (n = 55). The general applicability of the multi-modal drifter is field-tested, and the repeatability of each of the sensor time series is determined. Finally, we investigate the potential of the proposed multi-modal drifter to measure the surface transport velocity along a supraglacial channel flow path, and critically assess the device's performance for glaciological applications. As the sensing drifters used here are for the first time employed in a glacial environment, our study aims at characterizing sensor performance and suitability, rather than already coming up with detailed glaciological data interpretations.

Table 1: Overview of subsurface glaciology sensing platforms reported in the literature.

Paper	Measured parameters	Deployment	Communication	Lifetime	Published data?	Study purpose	Additional information

https://doi.org/10.5194/tc-2019-132
Preprint. Discussion started: 8 July 2019

Martinez et al. (2004)	Orientation, pressure, temperature	Borehole	Wireless, 433 MHz	Short-term	Yes	Development of sensor network	Glacsweb project
Hart et al. (2006)	Pressure, tilt angle, temperature, resistivity, strain gauge	Borehole	Wireless 433 MHz	One year	Yes	Clast transport	Installed in sediment, Glacsweb project
Behar et al. (2009)	Pressure, temperature, 3D acceleration	Moulin	Iridium	Short-term	No	Conference Abstract/ Sensor development	Platform lost during deployment
Rose et al. (2009)	Temperature, pressure, resistance, tilt	Borehole	Wireless, 173 MHz	One year	Yes	Basal conditions	Glacsweb project
Hart et al. (2011a)	Temperature, water pressure, probe deformation, conductivity, tilt	Borehole	Wireless, 173 MHz	One year	Yes	Till behaviour	Glacsweb project
Hart et al. (2011b)	Water pressure, probe deformation, conductivity, temperature	Borehole	Wireless, 173 MHz	1-2 years	Yes	Investigation of glacier break-up	Glacsweb project
Bagshaw et al. (2012)	Radio beacon, pressure	Moulin	Wireless, 151 MHz	Short-term	Yes	Drifter development	Only feasibility test of drifters, stationary pressure recordings

https://doi.org/10.5194/tc-2019-132
Preprint. Discussion started: 8 July 2019

Smeets et al. (2012)	Water pressure	Borehole	Wireless, 30 MHz	10 years	Yes	Subglacial pressure	Wireless transfer through up to 2500 m ice thickness
Lishman et al. (2013)	Acoustic attenuation	Borehole	Wireless, different frequencies	Short-term	Yes	Acoustic communication through ice	30 kHz predicted to be most feasible frequency for communication
Bagshaw et al. (2014)	Pressure	Moulin	Wireless, 151 MHz/ 433 MHz	Short-term	Yes	Development of drifters	Stationary Cryoegg
Bagshaw et al. (2014)	Pressure, temperature, conductivity	Moulin	Wireless, 151 MHz/ 433 MHz	Short-term	Yes	Development of drifters	ETracer drifter
Hart et al. (2015)	Temperature, water pressure, probe	Borehole	Wireless, 173 MHz	One year	Yes	Study subglacial/ englacial waterflow	Glacsweb project
van de Wal et al. (2015)	Pressure	Borehole	Wireless, 30 MHz	One year	Yes	Ice velocities	Platform from Smeets et al., 2012
How et al. (2017)	Pressure, temperature, tilt	Borehole	Wireless, 30 MHz	7-14 months	Yes	Subglacial hydrology	Platform from Smeets et al., 2012
Martinez et al. (2017)	Passive seismics, 3D acceleration, digital compass, temperature	Borehole	Cabled/ Wireless, 173 MHz	Short-term deployment	Yes	Glacier stick-slip	Fixed location Geophones, Glacsweb project

https://doi.org/10.5194/tc-2019-132
Preprint. Discussion started: 8 July 2019

Bagshaw et al. (2018)	Pressure, conductivity, temperature	Borehole	Wireless, 151.6 MHz	3 months	Yes	Subsurface firn/ snow studies	Merged Cryoegg and ETracer platform
Hart et al. (2019)	Pressure, stress, conductivity, tilt, temperature	Borehole	Wireless, 173 MHz	Up to 2 years	Yes	Glacier stick-slip motion, till deformation	Glacsweb project
This study	Pressure, acceleration, magnetic field, spinning rate, Euler angels	Moulins, meltwater channels	WiFi, after recovery	Short-term	Yes	Drifter proof-of-concept and data repeatability assessment	Reliability study, time series feature detection

https://doi.org/10.5194/tc-2019-132
Preprint. Discussion started: 8 July 2019

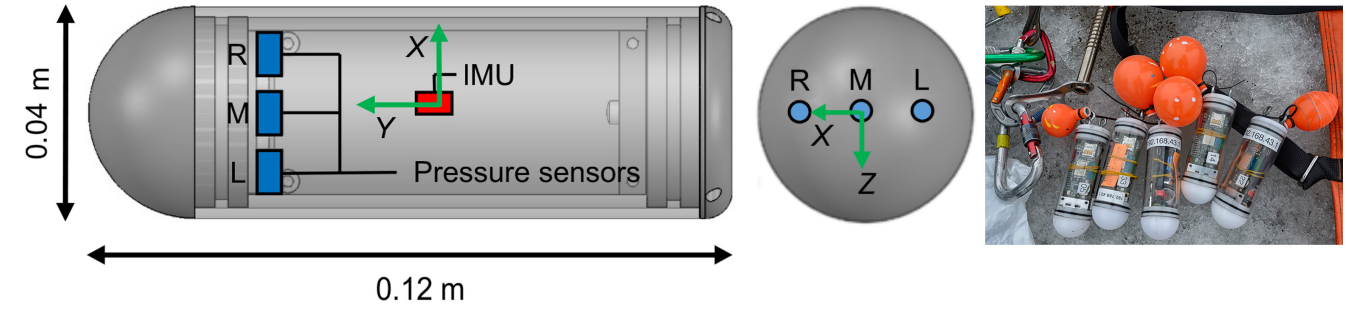

Figure 1. Schematic and dimensions of the multi-modal drifter used in this work showing the locations of the three pressure transducers and the inertial measurement unit (IMU). Left: Side-view of the drifter. Middle: Top-view facing the cap showing the left (L), middle (M) and right (R) pressure holes. Right: Drifters on the glacier surface shown with attached balloons used for manual buoyancy adjustment.

2 Methods

2.1 Multi-modal drifter

The drifter platform used in this study has a housing consisting of two POM plastic end caps and a 4 cm outer diameter polycarbonate plastic tube, with a total length of 12 cm, and mass of 143 g. Neutral buoyancy of the drifter is achieved by manually adjusting the length of the sensor by screwing the flat end cap inwards or outwards to modify the total volume. Balloons can additionally be attached to the drifter, to further adjust the buoyancy, as seen in the right panel of Figure 1. Balloons are used during the field deployment of this study. Each hemispherical end cap of the drifters contains three digital total pressure transducers. The 2 bar span transducer (MS5837-2BA, TE Connectivity, Switzerland) are programmed with a sensitivity of 0.0021 kPa (0.21 mm water column). They are linearly rated for 25 m of water depth, and can be used up to 45 m of water depth using a non-linear correction based on laboratory calibration. Each pressure transducer is equipped with its own on-chip temperature sensor, allowing for all pressure readings to include real-time temperature correction using a 2nd order correction algorithm.

All drifter units are equipped with an atmospheric auto-calibration algorithm. Once the devices have been activated using a magnetic switch, data from each pressure transducer is logged for 15 seconds. The atmospheric pressure, including the sensor-specific offset, is recorded internally. Afterwards, all three transducers are set to a default value of 100 kPa at local atmosphere. All sensors are therefore auto-calibrated to local changes in atmospheric pressure, which occur during the day, directly before each field deployment. This feature removes the necessity of manually correcting pressure sensor readings. The drifter units use three pressure sensors (marked as Left, Middle and Right in Figure 1), and can be outfitted with either 2 bar or 30 bar sensors, as opposed to a single pressure sensor providing triple modular redundancy by including a pressure sensor array in lieu of a single pressure sensor. The middle pressure sensor was however not used in this study due to the lower sensitivity and range of pressures experienced during channel passage. All following work will therefore only refer to the two lateral (left

https://doi.org/10.5194/tc-2019-132
Preprint. Discussion started: 8 July 2019

Table 2. Overview of the drifter text file data format. Each of the 27 columns corresponds to a different variable saved during channel passage at 100 Hz (magnetometer 20 Hz), units given in parentheses.

Col 1	Col 2	Col 3	Col 4	Col 5	Col 6	Col 7	Col 8	Col 9
Timestamp (ms)	Pressure left (hPa)	Left temp (°C)	Pressure center (hPa)	Center temp (°C)	Pressure right (hPa)	Right temp (°C)	Euler angle X (deg)	Euler angle Y (deg)
Col 10	Col 11	Col 12	Col 13	Col 14	Col 15	Col 16	Col 17	Col 18
Euler angle Z (deg)	Quat. X (-)	Quat. Y (-)	Quat. Z (-)	Quat. W (-)	Magnet. X (µT)	Magnet. Y (µT)	Magnet. Z (µT)	Dynamic linear accel. X ($m\,s^{-2}$)
Col 19	Col 20	Col 21	Col 22	Col 23	Col 24	Col 25	Col 26	Col 27
Dynamic linear accel. Y ($m\,s^{-2}$)	Dynamic linear accel. Z ($m\,s^{-2}$)	Rate gyro X ($rad\,s^{-1}$)	Rate gyro Y ($rad\,s^{-1}$)	Rate gyro Z ($rad\,s^{-1}$)	Calibration status magnet. (0-3)	Calibration status accel. (0-3)	Calibration status gyro. (0-3)	Sum calibration status (0-9)

and right) pressure sensors. In addition to the three pressure transducers, the drifter platform also contains a digital 9 degree of freedom (DOF) inertial measurement unit (IMU) (BNO055, Bosch Sensortec, Germany) integrating linear accelerometer, gyroscope and magnetometer sensors. The device uses proprietary (Bosch Sensortec) sensor fusion algorithms to combine the linear accelerometer, gyroscope and magnetometer readings into the body-oriented Euler angles to provide real-time absolute orientation at 100 Hz. These IMU sensors were chosen as they represent the current state-of-the-art in IMU technology. Additionally, they have the further benefit that the real-time calibration status of each of the three sensors is recorded (0, lowest to 3, highest) as part of each data set in order to provide quality control information for all IMU measurement data. When running in sensor fusion mode, all variables are saved at 100 Hz, with the exception of the magnetometer, which is recorded at a maximum rate of 20 Hz. Vibration and destructive testing of the IMU have additionally been conducted up to 3000 times the gravitational acceleration, thus showing that the drifter platform is suitable for deployment under harsh conditions.

The IMUs were configured to read out more data in addition to the dynamic linear acceleration (body acceleration due to external forcing only, gravity vector removed) and rate of angular rotation (rate gyro), relative to the x-, y- and z-axes of the sensor, as shown in Figure 1. The additional data include the real-time calculation of the drifter body-orientation (3D Euler angles relative to x-, y-, and z-axes and the angles as Quaternions) as well as the 3D magnetic field vector. The orientation of the vector measurements of the magnetometer readings correspond to the axes of the sensor which are identical to the accelerometer and rate gyro axes. All drifter sensor data is saved as a 27 column ASCII text file with the structure listed in Table 2. The text files were transferred from the drifters via Wifi to a field computer after drifter recovery from the stream.

https://doi.org/10.5194/tc-2019-132
Preprint. Discussion started: 8 July 2019

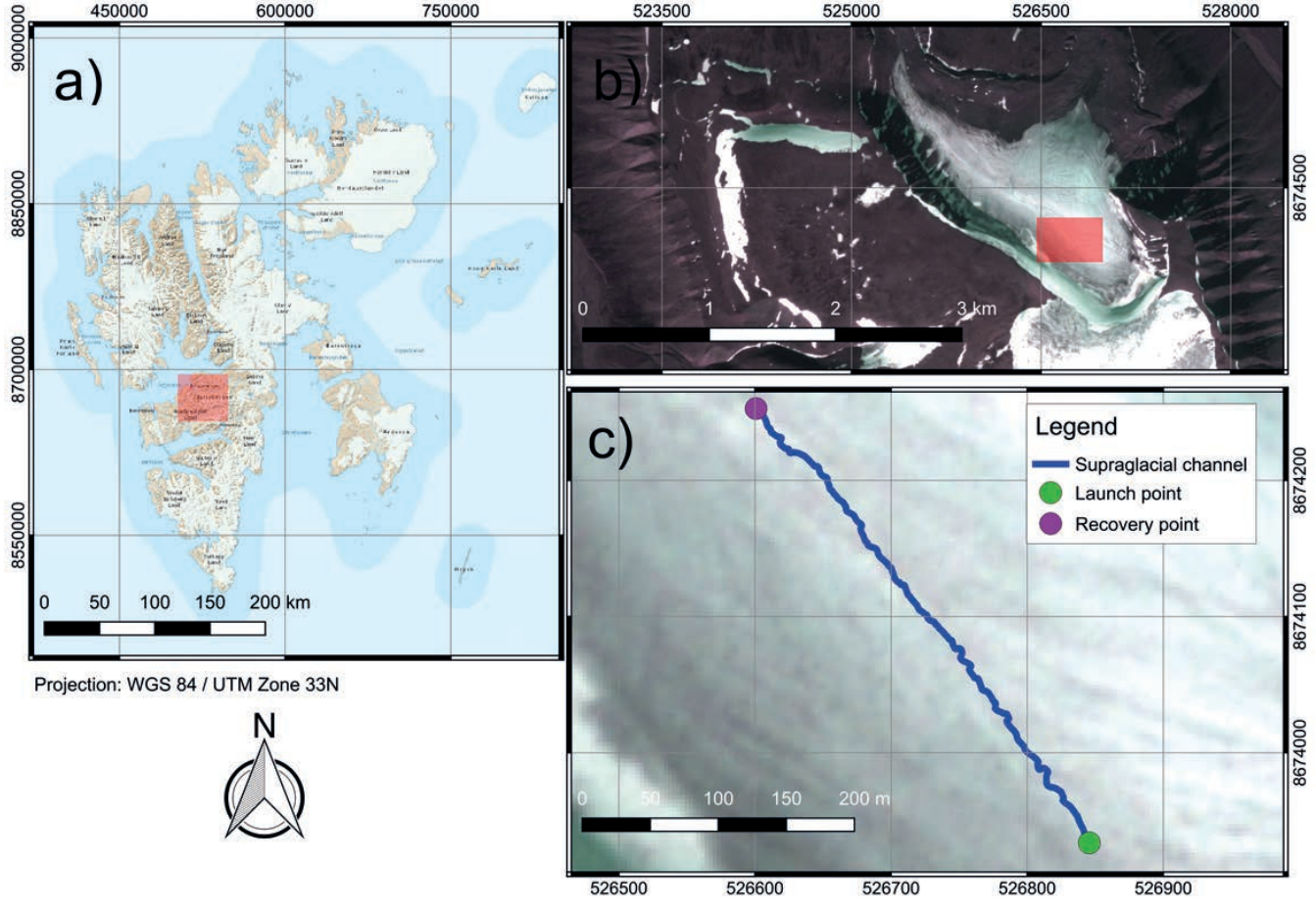

Figure 2. a) Location of the Foxfonna glacier on the Svalbard archipelago. Basemap: © Norwegian Polar Institute. b) PlanetScope false color overview of the Foxfonna glacier and the location of the investigated supraglacial channel acquired on 01.08.2018. c) Close up of the studied supraglacial channel. Background image from PlanetScope acquired on 01.08.2018.

2.2 Study site

Fieldwork for this study was conducted between 04.08 and 07.08.2018 on the small valley glacier Foxfonna, located on the main island of the Norwegian Arctic archipelago Svalbard. The cold-based, roughly 2.9 kilometers long glacier is located on a northwest-facing slope between 330 and 750 meters elevation above sea level at the end of the Adventdalen valley, next to the main settlement at Longyearbyen. The glacier has a network of supraglacial channels developing on the surface of the glacier during summer time. Some of the channels either cut deep enough to form englacial cut-and-closure systems (Gulley et al., 2009) or they are still partly snow-plugged during summer time. Additional channels emerge at the glacier front, indicating existing subglacial drainage channels.

https://doi.org/10.5194/tc-2019-132
Preprint. Discussion started: 8 July 2019

2.3 Field Deployments

Two different experiments were conducted on the glacier surface. The first experiment tested the general feasibility of the drifters to travel through an englacial/subglacial system and to be successfully recovered. The first experiment involved deploying five wooden drifter surrogates identical in size to our multi-modal drifters in a 2.5 km long supraglacial, partly englacial channel. The channel on the eastern side of the glacier had several well-developed step-pool sequences and was incised deeply into the glacial ice. Further downstream, the channel developed into a partly snow-plugged, partly englacial system. The final channel section had a high amount of debris, representative of subglacial environments. A net was installed where the channel reemerged on the surface at the eastern lateral moraine. Reemerging dummies were trapped in the net and recovered.

The second, main experiment was conducted along a 450 m section of a Foxfonna supraglacial channel. The investigation section had a total elevation difference of 30 meters (handheld GPS accuracy of 5 meters) as measured between the start and the end of the channel section. The section included several step-pool sequences as well as rapids and recirculation zones. The experiments were conducted within this channel section for three principle reasons. First, the purpose of the study was to determine field measurement repeatability, requiring a channel with different morphological features. Second, with only five prototypes, the risk of losing a drifter had to be kept low. Finally, the study of the supraglacial system allowed for the filming of deployments, and this provides a simple and robust evaluation method to compare the sensor data with observed movements of the drifter within the flow. All five drifters were launched from the green marked location on the map in Figure 2, and were recovered using a marine fishing net, installed at the downstream end of the channel section. A total of 55 drifter deployments with five multi-modal drifters were conducted. 10 deployments were collected in the afternoon of the second field day (05.08.2019 15:52 -17:20 local time) and the remaining 45 deployments in the late evening and night of the fourth field day (07.08.2019 18:53 – 23:37 local time). It must be stated that the discharge varied throughout the deployment time, depending largely on weather conditions (sunny, with increased melt on 05.08 and cloudy, rainy, sunny on 07.08). Some of the deployments had slightly varying buoyancy, due to varying balloon inflation, but all deployments on the 450 m section were conducted with a single balloon. Four out of the fifty-five deployments had the drifters connected in tandem with cable ties, to test the variation between the sensor readings of two different drifters passing through nearly identical flow paths. All of the drifters were switched on and then left on the ground for at least 30 seconds before deployment and for an additional 30 seconds after successful recovery from the stream and before switching off. This was done to ensure that the drifters had enough time for self-calibration to atmospheric pressure before the deployment and the IMU sensor readings could calibrate and provide constant-value readings, which later serve to mark the start and stop of each deployment.

2.4 Data preparation and processing workflow

All data processing was performed using Matlab R2018b. Corrupted datasets with missing data or faulty sensor readings were removed. In cases where a drifter switched off and back on during a deployment, multiple files were concatenated into a single

https://doi.org/10.5194/tc-2019-132
Preprint. Discussion started: 8 July 2019

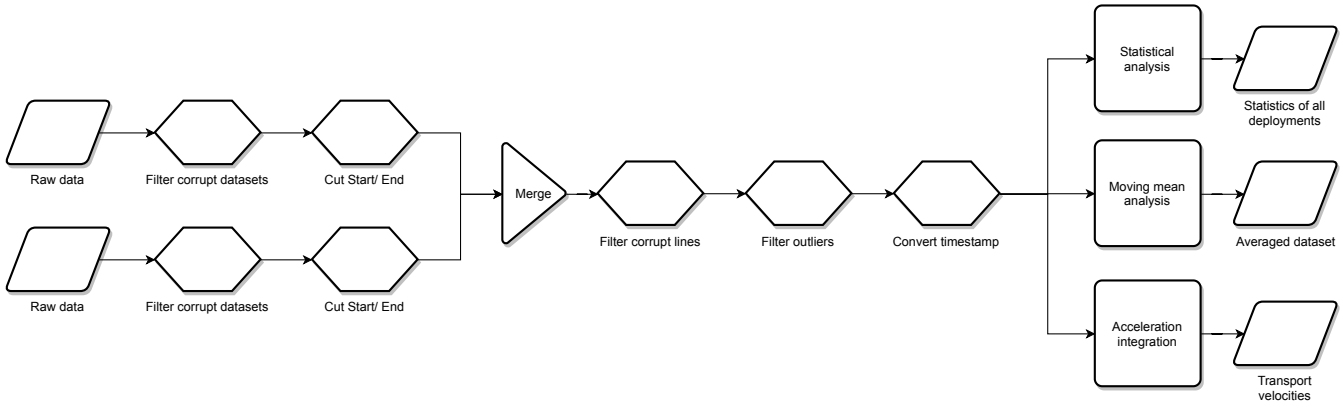

Figure 3. Overview over the multi-modal drifter data post-processing workflow.

dataset. The start and end of each dataset were manually trimmed such that that the processed time series only represent the time within the glacial stream. Threshold criteria used for determining the start of measurement were the linear acceleration peaks of a drifter's first impact with the water surface during deployment as well as the final impact when the drifter contacted the net during recovery. Lines in the dataset with no data or poor calibration status were filtered out in the next step. After trimming, the time series data were filtered for outliers with the following thresholds: $\pm 200\,\mu\mathrm{T}$ for the magnetometer, $\pm 60\,\mathrm{m\,s^{-2}}$ for the linear accelerometer and $\pm 50\,\mathrm{deg\,s^{-1}}$ for the rate gyro.

The statistical analysis evaluated the degree of agreement between individual sensor time series for each deployment to assess the repeatability of the drifter field data. Pearson product-moment correlation coefficients were used to investigate the correlation structure between different sensor modalities, and to assess if the different modalities were dependent or independent variables. In the next step, the empirical probability distributions were investigated together with the statistical moments mean, variance, standard deviation, skewness and kurtosis. Afterwards, the empirical probability distributions of each deployment were compared to the ensemble empirical probability distributions to determine the measurement repeatability. To ensure a robust assessment of repeatability, several criteria were evaluated: chi square distances, mean absolute error, mean squared error, data ranged normalized root mean square and the Kullback Leibler divergence (Kullback and Leibler, 1951).

The assessment of the minimum needed sample size to achieve a given precision of each mode (e.g. total pressure, linear acceleration in the x – direction) was done following the equation from Hou et al. (2018)

$$n = \frac{Z^2_{1-\frac{\alpha}{2}}}{\varepsilon^2} \cdot \left(\frac{\sigma}{\mu}\right)^2 \tag{1}$$

where $Z^2_{1-\frac{\alpha}{2}}$ is the standard normal deviate (e.g. $Z_{0.975} = 1.96$ for the 95% confidence interval), ε is the defined precision, σ is the standard deviation of the population and μ is the population mean. In this study, we defined the sample mean to be within ±10% of the true value (i.e. $\varepsilon = 0.10$), 95% of the time (i.e. $Z_{0.975} = 1.96$). The values for σ and μ were then obtained from

https://doi.org/10.5194/tc-2019-132
Preprint. Discussion started: 8 July 2019

the statistical analysis of the time series data from all deployments.

To find potential features in the time-series and to test if the recorded data is varying over time, moving means were calculated over the dataset. The moving means for this study were calculated over a time window of five seconds, as potential signal features were most prominent at this window length, and plotted together with the 95% confidence interval. This was done for forty of the deployments (n=40) for the first 200 seconds of the channel passage. The analysis was limited to the first 200 seconds, as not all drifters recorded for the full length of time, so that a compromise had to be found between getting as many deployment datasets as possible with an as long time span possible at the same time. The other 15 deployments out of the total 55 deployments were left out as they either recorded no data (n=9) or recorded only for parts of the passage (n=6) leading to very short datasets.

The surface transport speed was calculated by integrating the acceleration measurements over a rolling time window for the remaining 40 deployments (n=40). The window width was in an initial step randomly chosen for the velocity calculation. Once the three components of the velocity vector were calculated, we defined the transport speed as the magnitude of the velocity. The transport speed was then compared to the estimated transport velocity, which was found by dividing the transport distance (450 m) by the total travel time of the drifter. The integration window size was then readjusted individually for every deployment, so that it would be within a 10% error threshold from the drifter's estimated transport velocity. By doing so, the individual changes in the observed transport velocity are accounted for. As the acceleration includes rapid changes in rigid body motion, for instance due to impact with the channel walls, we found that integration produced large outliers, which are not representative of the water flow itself. Therefore the estimated instantaneous velocities, whose absolute values exceeded $10\,\mathrm{m\,s^{-1}}$, were filtered.

3 Results

3.1 Utility rate

In the first experiment, five wooden dummies were deployed in a 2.5 km long supraglacial, partly englacial channel with features of subglacial channels, and four out of five dummies were recovered after 72 hours. The second experiment consisted of 55 multi-modal drifter deployments in a 450 m supgraglacial channel section, returning a total of 40 useful datasets. The other 15 deployments had either too short datasets (below 200 seconds, compared to an average transit time of 360 seconds), as drifters only recorded part of the deployments there or recorded no data at all. This leads to the definition of a recovery and a utility rate for the drifter deployments:

$$\text{Recovery rate} = \frac{\text{Number of recovered dummies/ drifters}}{\text{Number of deployed dummies /drifters}}. \quad (2)$$

https://doi.org/10.5194/tc-2019-132
Preprint. Discussion started: 8 July 2019

$$\text{Utility rate} = \text{Recovery rate} \cdot \text{Data usability rate} = \frac{\text{Number of recovered dummies/ drifters}}{\text{Number of deployed dummies/ drifters}} \cdot \frac{\text{Number of usable datasets}}{\text{Number of recovered drifters}} \quad (3)$$

Supraglacial system from the second experiment with 5 drifters and a total of 55 deployments in 450 m long supraglacial channel:

Recovery rate $= \frac{55}{55} = 1.00$,
Utility rate $= \frac{55}{55} \cdot \frac{40}{55} = 0.73$.

Subglacial/englacial system from the first experiment with 5 dummies in 2.5 km long channel:

Recovery rate $= \frac{4}{5} = 0.80$.

Estimated total utility rate for **subglacial/englacial** deployments:

Utility rate $= \frac{4}{5} \cdot \frac{40}{55} = 0.58$.

3.2 Empirical probability density distributions

Empirical probability density distributions in combination with ensemble statistics allow a simple overview of each dataset, the distribution of a parameter's values and their variability. Figure 4 shows the empirical probability density distributions of all successful deployments (n=40) and all sensor records as well as the IMU calculations for Quaternions and Euler angles. Additionally, the normal distribution fitted to each dataset is plotted as a red line. Both the visual interpretation of the empirical probability distributions in Figure 4 as well as the mean values in Table 3 strongly indicate that the values for the acceleration, rate gyroscope and the quaternions are close to zero, meaning the drifters remained nearly motionless for long periods of time during measurement. This is due to many of the drifters being stuck in the channel for several minutes before they were dislodged and carried further by the current.

The skewness of the distributions indicates the asymmetry of the data around the origin. It therefore assess whether a dataset is symmetric or if it is deviating from a central tendency. The pressures, magnetometer in the y-direction, gyroscope in the x-direction and the Euler angles in both the x- and y-directions are slightly skewed towards values above the mean. The acceleration in the y-direction is more skewed towards positive values due to the orientation (facing down and into the direction of motion) of the drifter as it was advected by the flow. All other sensor readings are more skewed in the negative direction from the mean.

A kurtosis of value 3 indicates distribution similarity to a Gaussian distribution. The left pressure sensor readings, magnetometer in x-direction and the Euler angles in the y- and z-directions exhibit a kurtosis, which is nearly Gaussian. All other sensor readings were found to be non-Gaussian. The accelerations had high kurtosis values, this can clearly be seen in Figure

https://doi.org/10.5194/tc-2019-132
Preprint. Discussion started: 8 July 2019

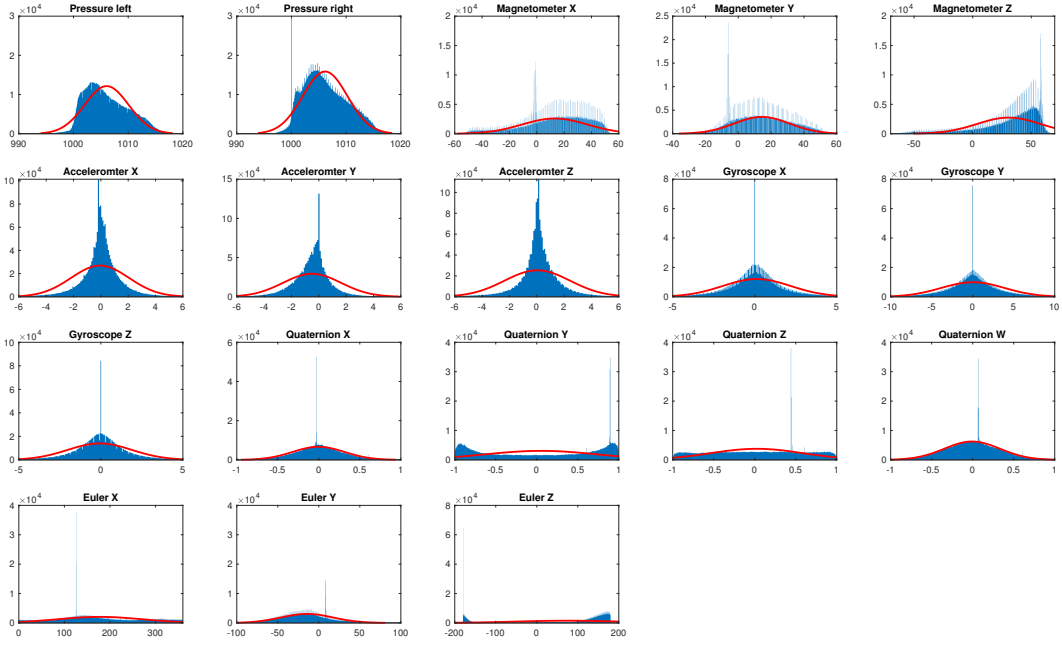

Figure 4. Empirical probability distributions of 40 deployments (n=40) of the recorded sensor data in blue with a normal fit in red.

4 and is, again, caused by longer periods where the drifters were stranded in shallow regions or stuck within the channel and did not move for several minutes.

The mean values and the standard deviations from Table 3 were used to estimate the required sample size to achieve a precision of the sample mean to be within ±10% of the true value (i.e. $\varepsilon = 0.10$) for 95% of the time (i.e.$Z_{0.975} = 1.96$). The obtained sample size estimates were afterwards multiplied with the utility rates to estimate the required number of supraglacial and subglacial/englacial deployments. The mean pressure values were thereby corrected with the calculated air pressure of 941.8 hPa based on elevation (600 m) and air temperature on 07.08.2018. As Table 4 shows, the required sample sizes are unrealistically high. These high numbers are however not necessarily an indicator of sensor accuracy, but rather an indicator of spatial and temporal flow variability. The lowest required sample size was for the pressure sensors and the magnitude of the magnetometer. The latter should however also be corrected by the value of the local magnetic field strength and the number of required deployments is therefore likely to be higher.

https://doi.org/10.5194/tc-2019-132
Preprint. Discussion started: 8 July 2019

The Cryosphere Discussions

Table 3. Ensemble statistics of all multi-modal time series: mean, variance, standard deviation, skewness and kurtosis.

Sensor mode	mean	variance	standard deviation	skewness	kurtosis
Pressure left	1006.05 hPa	16.19 hPa^2	4.02 hPa	0.45	3.11
Pressure right	1006.15 hPa	16.69 hPa^2	4.09 hPa	0.38	3.45
Magnetometer X	13.14 µT	567.70 $µT^2$	23.83 µT	−0.62	2.83
Magnetometer Y	14.35 µT	284.65 $µT^2$	16.87 µT	0.17	2.28
Magnetometer Z	30.78 µT	729.40 $µT^2$	27.01 µT	−1.33	4.23
‖Magnetometer‖	53.76 µT	17.63 $µT^2$	4.20 µT	−0.30	3.09
Accelerometer X	−0.06 $m\,s^{-2}$	4.48 $m^2\,s^{-4}$	2.12 $m\,s^{-2}$	−0.95	94.84
Accelerometer Y	−0.49 $m\,s^{-2}$	4.52 $m^2\,s^{-4}$	2.13 $m\,s^{-2}$	4.53	218.62
Accelerometer Z	0.04 $m\,s^{-2}$	5.78 $m^2\,s^{-4}$	2.40 $m\,s^{-2}$	−1.75	124.54
‖Accelerometer‖	2.34 $m\,s^{-2}$	9.54 $m^2\,s^{-4}$	3.09 $m\,s^{-2}$	7.55	102.39
Gyroscope X	0.12 deg s^{-1}	4.32 $deg^2\,s^{-2}$	2.08 deg s^{-1}	0.58	10.31
Gyroscope Y	0.02 deg s^{-1}	14.88 $deg^2\,s^{-2}$	3.86 deg s^{-1}	−0.10	8.18
Gyroscope Z	−0.07 deg s^{-1}	3.83 $deg^2\,s^{-2}$	1.96 deg s^{-1}	−0.41	11.22
‖Gyroscope‖	3.65 deg s^{-1}	9.73 $deg^2\,s^{-2}$	3.12 deg s^{-1}	2.20	11.59
Quaternion X	−0.003	0.10	0.32	−0.02	3.68
Quaternion Y	0.05	0.48	0.69	−0.12	1.48
Quaternion Z	0.02	0.31	0.56	−0.09	1.88
Quaternion W	−0.006	0.12	0.34	−0.01	3.35
Euler X	177.47 deg	8599.48 deg^2	92.73 deg	0.20	2.16
Euler Y	−14.42 deg	1008.31 deg^2	31.75 deg	0.41	3.18
Euler Z	75.68 deg	15,963.50 deg^2	126.35 deg	−1.26	2.91

3.3 Statistical evaluation

Distance and similarity measures were used to test the repeatability of the datasets. The probability density distribution of each time series data set was compared with the ensemble probability density distributions of all data sets. Various measures can then give an indication on how much the two compared probability density distributions equal each other, meaning how similar they are. Zero values indicate that the distributions are similar and that the experiment is repeatable. For this study, the Chi Squared Error, the Kullback Leibler divergence (KLD), mean average error, the mean squared error and the data range normalized root mean square were calculated for every sensor modality and direction (n = 40). The results are provided in Table 5. The values are generally very low, indicating that the empirical probability density distributions of the single deployments do not deviate much from the probability density distributions of the whole dataset. The highest KLD values are the ones of the right pressure, the magnetometer in x- and z-direction, the acceleration in y-direction and the quaternions in w-direction. The

https://doi.org/10.5194/tc-2019-132
Preprint. Discussion started: 8 July 2019

Table 4. Estimated multi-modal sample sizes for ±10% precision and a 95% confidence interval based on measured mean values and standard deviations from all deployments (n=40), as well as estimated sample sizes for supraglacial and subglacial deployments based on the utility rate and the measured mean values and standard deviations.

Sensor mode	Estimated sample size	Supraglacial	Subglacial
Pressure left	2	3	4
Pressure right	2	3	4
Magnetometer X	1264	1732	2180
Magnetometer Y	531	728	916
Magnetometer Z	296	406	511
‖Magnetometer‖	3	4	5
Accelerometer X	479,603	656,991	826,902
Accelerometer Y	7259	9944	12,516
Accelerometer Z	1,382,976	1,894,488	2,384,442
‖Accelerometer‖	670	918	1155
Gyroscope X	115,419	158,109	198,999
Gyroscope Y	14,309,576	19,602,159	24,671,683
Gyroscope Z	301,182	412,578	519,280
‖Gyroscope‖	281	385	485

values are however still very close to zero, thus indicating a high repeatability of the drifter deployments.

3.4 Pearson correlation coefficients

Calculating the Pearson correlation coefficients between the different sensor datasets establishes potential correlations between the different sensor modalities and directions and can thus indicate if modalities are redundant or if they represent independent variables. To classify the associations, a modified classification scheme from Cohen (1992) was used. Thereby correlation coefficients from -1.0 to -0.9 and 0.9 to 1.0 were classified as very strong association. Coefficients from -0.9 to -0.5 and 0.5 to 0.9 as strong association, coefficients from -0.5 to -0.3 and 0.3 to 0.5 as moderate association, from -0.3 to -0.07 and 0.07 to 0.3 as weak association and correlation coefficients between -0.07 and 0.07 were classified as not associated. The resulting correlation coefficients together with their association classifications are shown in Figure 5. This figure confirms that the two pressure sensors are indeed redundant. The results also show an interesting correlation between the lateral pressure sensors and the magnetometer in the y-direction. A moderate negative association exists between the magnetometer in the y- and z-directions. The quaternions also have a moderate negative association between then x- and y-directions, and between the w- and y-/z-directions. Most sensor modalities represent statistically independent variables. The exceptions were the redundant signals from the two pressure sensors and the magnetometer in y-direction.

https://doi.org/10.5194/tc-2019-132
Preprint. Discussion started: 8 July 2019

Table 5. Ensemble statistical measures of comparison for all sensor modes. Shown are Chi Squared error (Chi), Kullback Leibler divergence (KLD), mean average error (MAE), mean squared error (MSD) and data range normalized root mean square (RMSD).

Sensor mode	Mean Chi	Mean KLD	Mean MAE	Mean MSD	Mean RMSD
Pressure left	1.9×10^{-4}	9.3×10^{-2}	-5.2×10^{-22}	1.4×10^{-7}	3.1×10^{-6}
Pressure right	1.3×10^{-2}	1.3×10^{-1}	1.5×10^{-21}	9.1×10^{-6}	9.6×10^{-6}
Magnetometer X	1.6×10^{-3}	2.5×10^{-1}	3.7×10^{-20}	1.5×10^{-6}	8.0×10^{-6}
Magnetometer Y	1.9×10^{-3}	1.4×10^{-1}	-2.7×10^{-20}	2.2×10^{-6}	8.0×10^{-6}
Magnetometer Z	1.3×10^{-3}	1.5×10^{-1}	3.3×10^{-20}	1.1×10^{-6}	5.5×10^{-6}
Accelerometer X	3.2×10^{-3}	3.6×10^{-2}	3.5×10^{-21}	1.4×10^{-5}	2.1×10^{-5}
Accelerometer Y	5.4×10^{-3}	1.0×10^{-1}	-5.6×10^{-20}	2.8×10^{-5}	3.4×10^{-5}
Accelerometer Z	3.9×10^{-3}	4.2×10^{-2}	-2.1×10^{-21}	2.0×10^{-5}	2.5×10^{-5}
Gyroscope X	5.5×10^{-3}	3.4×10^{-2}	-2.4×10^{-20}	3.8×10^{-5}	6.9×10^{-5}
Gyroscope Y	5.3×10^{-3}	5.7×10^{-2}	5.9×10^{-21}	1.9×10^{-5}	3.2×10^{-5}
Gyroscope Z	5.4×10^{-3}	3.8×10^{-2}	1.5×10^{-20}	3.8×10^{-5}	6.2×10^{-5}
Quaternion X	8.6×10^{-3}	6.8×10^{-2}	3.8×10^{-19}	5.5×10^{-4}	4.4×10^{-3}
Quaternion Y	8.3×10^{-3}	8.3×10^{-2}	-1.1×10^{-19}	4.4×10^{-4}	4.4×10^{-3}
Quaternion Z	6.2×10^{-3}	6.4×10^{-2}	-3.3×10^{-19}	3.2×10^{-4}	3.5×10^{-3}
Quaternion W	1.1×10^{-2}	1.0×10^{-1}	1.7×10^{-19}	6.4×10^{-4}	5.2×10^{-3}

3.5 Moving mean analysis

The moving mean analysis with a 5 second rolling time window filters out all short-term sensor fluctuations and leaves only major signal features, as it can be seen in Figure 6. The plot shows the records of the two lateral pressure sensors It is clearly seen that the signals of the two lateral pressure sensors are almost identical, creating a redundant signal.

As the experiments are conducted at atmospheric pressure conditions with only small elevation change over the passage, almost homogenous pressure signals should be expected. The plot in Figure 6 however, shows that the pressure records are displaying distinct variations including sharp peaks, sudden increases and drops. These variations are superimposed on a general increase of the pressure, which might be caused by the increasing atmospheric pressures as the drifters are flowing downhill, as well as increasing water depths in the channel. The 95% confidence interval of the averaged pressure signal can be seen to vary over time, but generally follows the same features as the average, with some features having smaller confidence intervals than others. The values of the 95% confidence intervals are generally very low and on average do not exceed values above ±0.11% of the mean pressure value of 1005 hPa.

https://doi.org/10.5194/tc-2019-132
Preprint. Discussion started: 8 July 2019

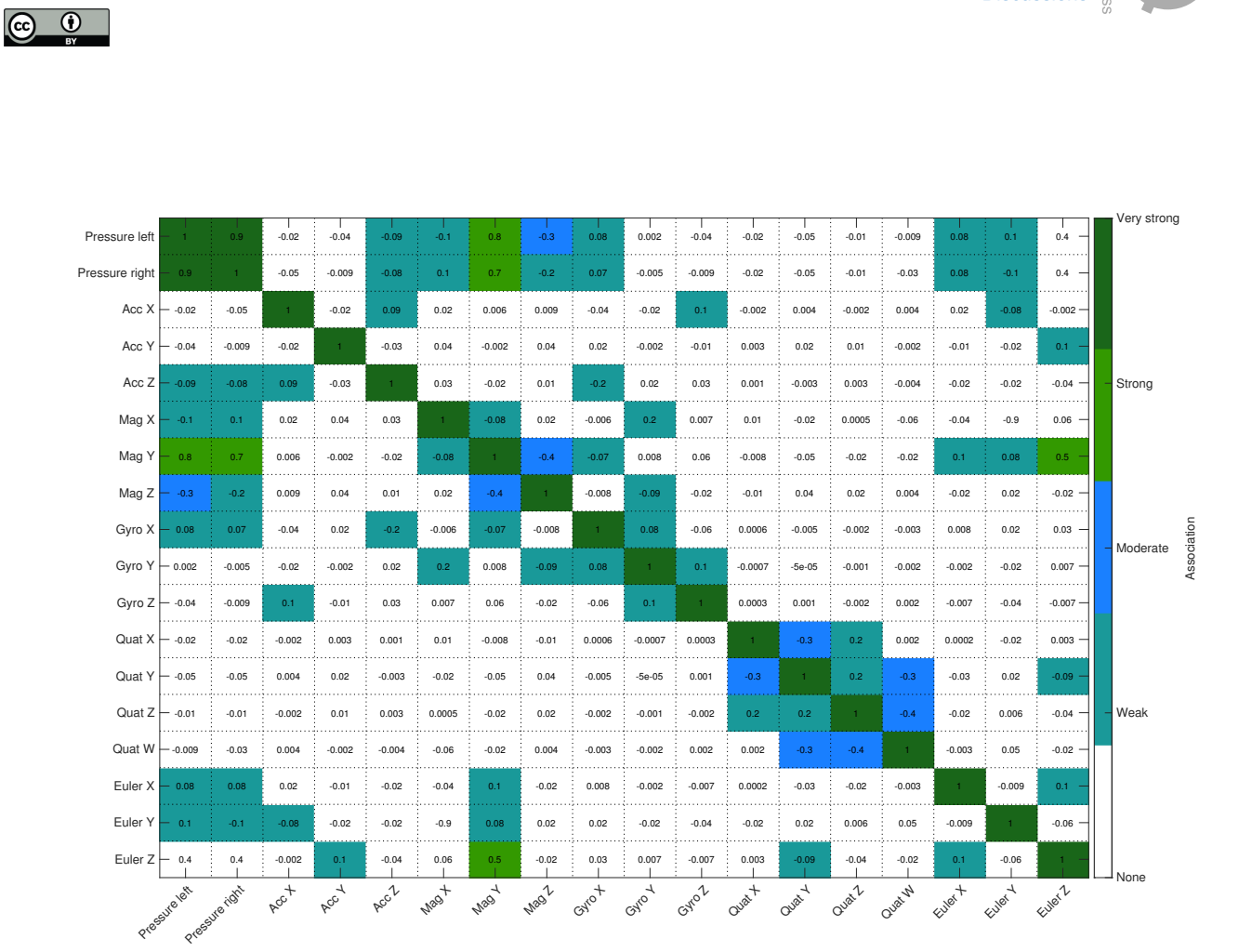

Figure 5. Pearson correlation coefficients (r) between the different sensor readings for all deployments (n=40). The classification is adapted after Cohen (1992).

Figure 7 shows a close correlation between the moving means of the left pressure and the magnetometer in the y-direction. The y-direction refers to the y-direction being aligned with the longitudinal axes of the drifter, which is most often oriented along the flow direction.

The next plot in Figure 8 shows the left pressure together with the magnitudes of the magnetometer, the gyroscope and the accelerometer averaged over a 5 second time window. Additionally the last panel shows the magnitude of the surface current speeds. All plots show that the obtained signals are not homogeneous over time, but rather have pronounced signal variations, and are also visible in the pressure signals.

https://doi.org/10.5194/tc-2019-132
Preprint. Discussion started: 8 July 2019

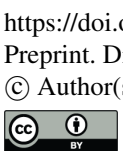

The Cryosphere
Discussions
Open Access
EGU

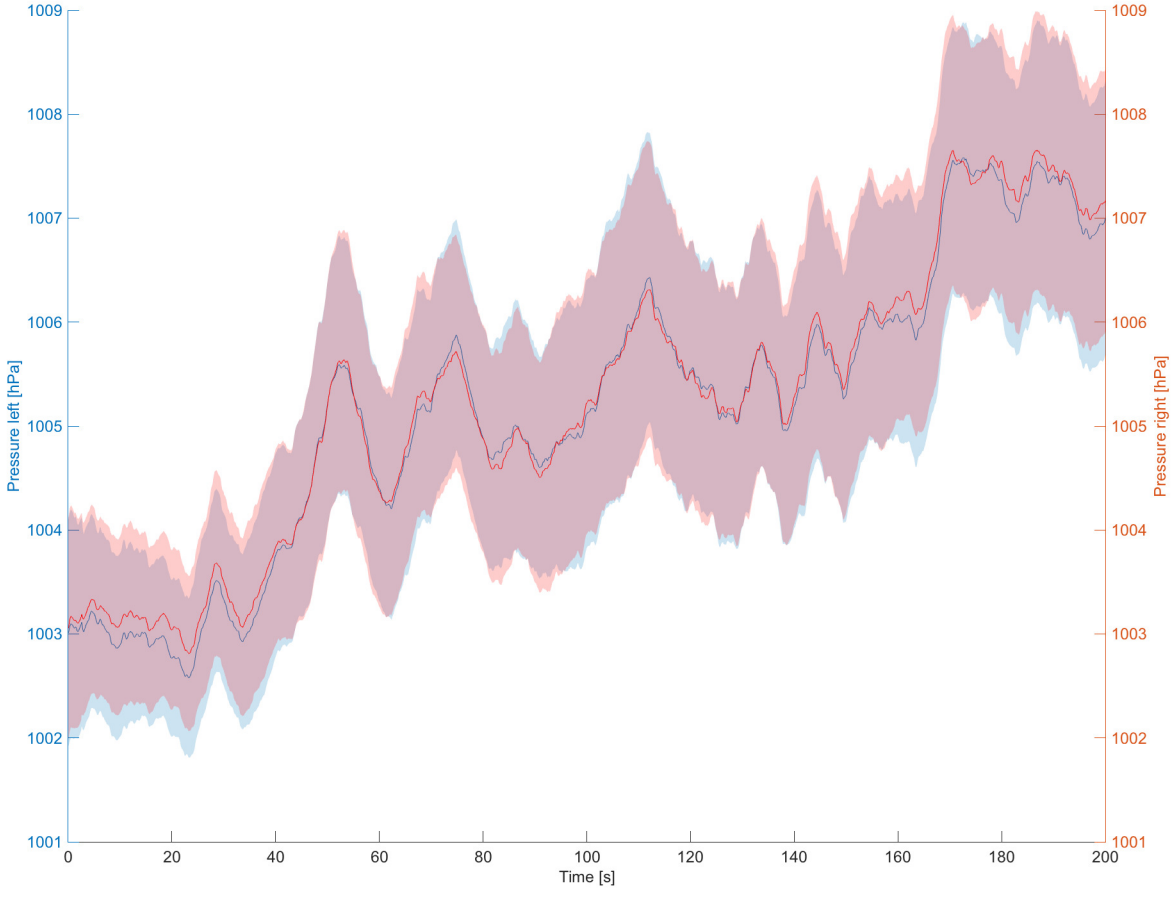

Figure 6. Mean values and 95% confidence interval (shaded area) of the left and right pressure over 40 deployments (n=40) over the first 200 seconds of the flow path passage. The data is averaged over a 5 s time window and across 40 deployments.

https://doi.org/10.5194/tc-2019-132
Preprint. Discussion started: 8 July 2019

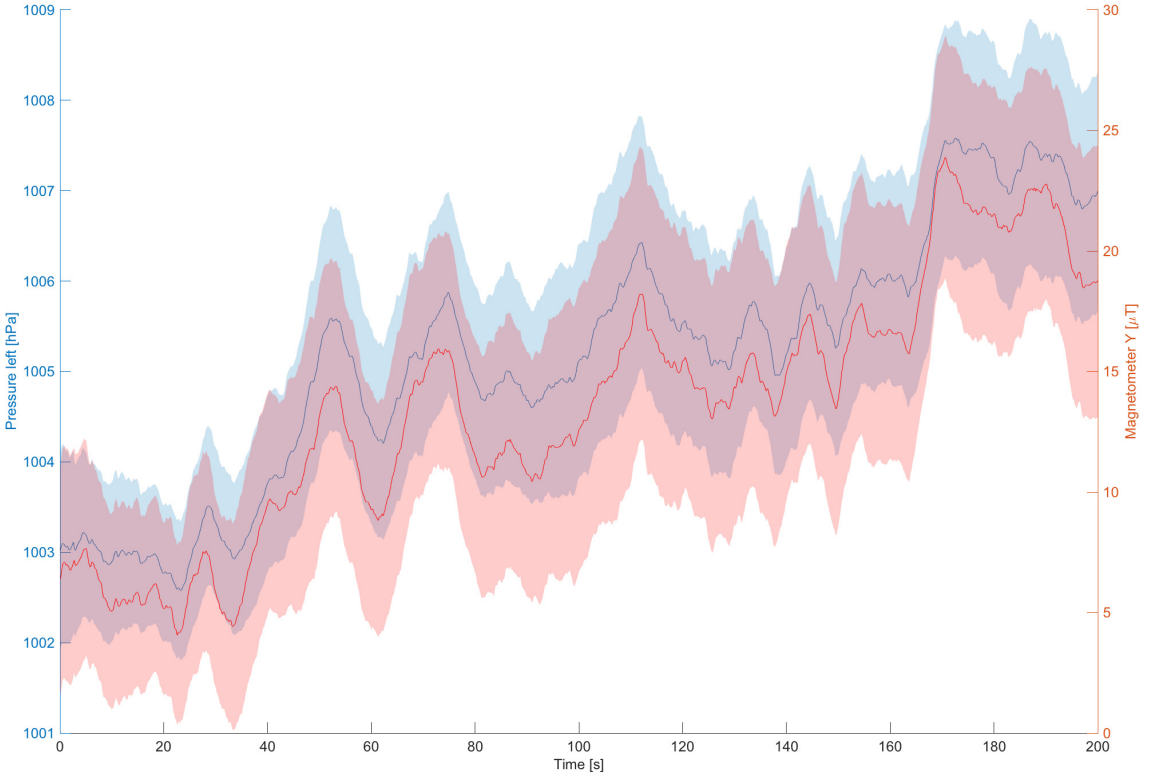

Figure 7. Left pressure and magnetometer in y-direction time series. The plot shows the first 200 seconds of 40 deployments (n=40), with a moving mean with a time window of 5 s and the 95% confidence interval (shaded area).

https://doi.org/10.5194/tc-2019-132
Preprint. Discussion started: 8 July 2019

The Cryosphere
Discussions
Open Access
EGU

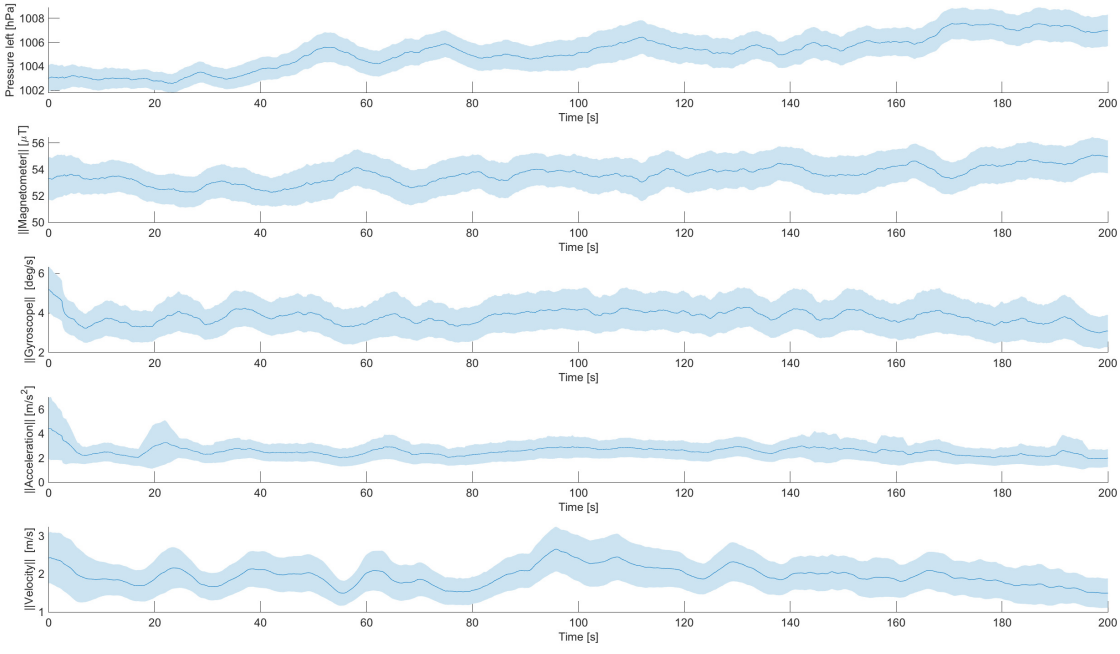

Figure 8. Left pressure overlayed with the magnitudes of the magnetometer, the gyroscope, the accelerometer and the velocities, obtained from acceleration integration. The line is the moving mean with a 5 s time window and the shaded area represents the 95% confidence interval of 40 deployments (n=40).

https://doi.org/10.5194/tc-2019-132
Preprint. Discussion started: 8 July 2019

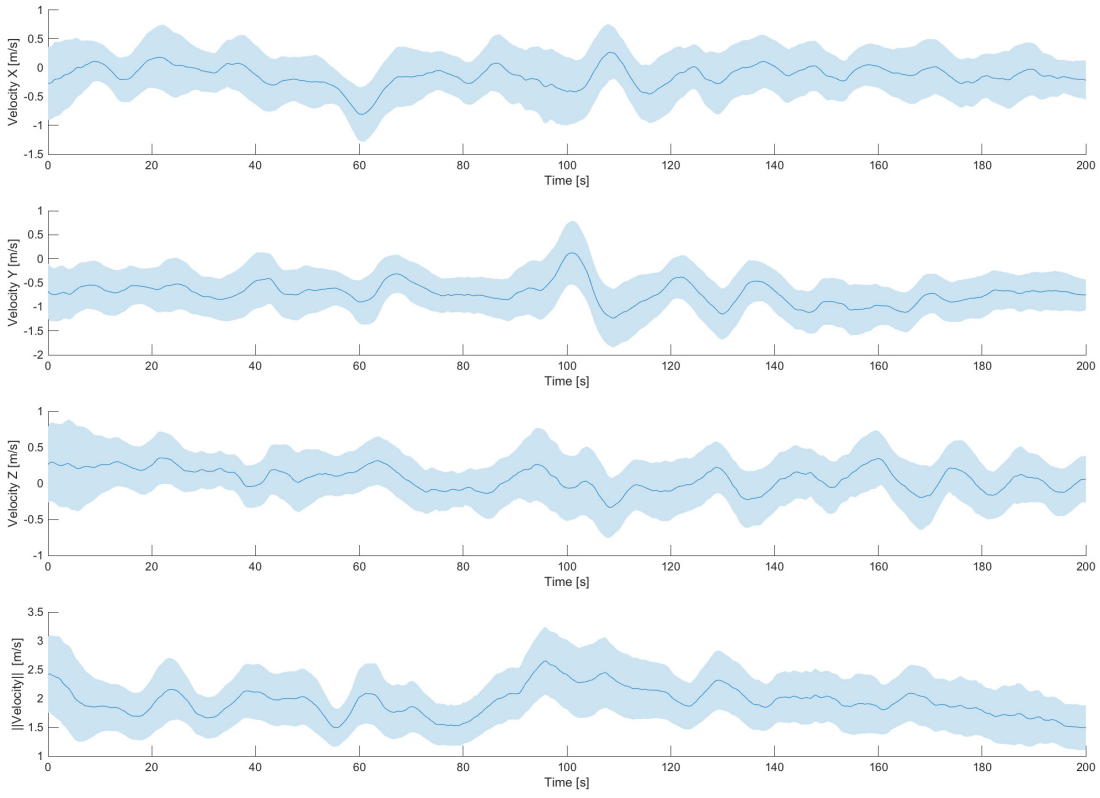

Figure 9. Mean values and 95% confidence interval of the three velocity components and velocity magnitude of 40 deployments (n=40) over the first 200 seconds of the flow path passage. The data is averaged over a 5 second time window.

The width of the confidence intervals of all sensor modalities decrease after drifter deployment, vary however slightly over the time series, as the drifters pass through different channel geometries and flow features at individual velocities. The magnitude of the magnetometer has the second smallest 95% confidence interval with a mean confidence interval of ±2.45% of its' mean value of 54.6 µT. The other sensor modalities have larger confidence intervals with gyroscope readings being the next lowest on the list with a mean confidence interval of ±24.8% of it's mean value of 3.8 deg s^{-1}. The accelerometer has the largest confidence interval, and hence largest variation of recorded values, with a mean confidence interval of ±34.4% of its' mean value of 2.54 m s^{-1}.

https://doi.org/10.5194/tc-2019-132
Preprint. Discussion started: 8 July 2019

3.6 Velocities

Integrating the three-dimensional accelerations provides the velocities, which were then filtered by taking the mean value over a 5 second window as shown in Figure 9. The velocities in the x-direction (sideways in the plane of the drifters longitudinal direction, see also Figure 1) alternate between positive and negative values as the drifters travel through a meandering channel. Velocities in the y-direction remained mostly negative and vary between fast and slow zones. The negative values in y-direction are due to the buoyancy adjustment of the drifter. Every drifter had one balloon attached (see right panel, Figure 1) to achieve neutral buoyancy. We observed that the currents lead to the balloon flowing slightly ahead and the drifter facing away most of the time, thus leading to negative accelerations and velocities in the y-direction (longitudinal direction of the drifter, see Figure 1). In the z-direction (downwards facing from the drifters longitudinal plane, see Figure 1) the velocities remained mainly positive and vary between zones with slower and faster flow.

The magnitude of the velocity shows several pronounced signal variations in the time series as well. Generally values around $2\,\mathrm{m\,s^{-1}}$ are most common. The mean value of the 40 deployments, used for acceleration integration, is $1.94\,\mathrm{m\,s^{-1}}$ and the mean 95% confidence interval is ±24.5% (n=40).

3.7 Signal features of a step-pool sequence

Video footage was taken periodically during the deployments, and supports the interpretation of the sensor records in terms of channel morphological features. Figure 10 shows the moving mean plot (2.5 seconds time window) of the left pressure sensor of one drifter during the passage of a small step-pool sequence, which was corroborated by video footage from the deployment.

The moving mean plot of the pressure shows a pronounced peak, followed by a drop in the signal for the chosen time period, where the drifter passed over the step-pool sequence. The video footage shows that the drifter was speeding up towards the edge of the step, when the pressure signal increased (Figure 10, A)). As the drifter flowed over the edge and dropped into the pool underneath, the pressure dropped. Once in the pool, the drifter was caught in a recirculating current and remained in the pool for several seconds. This leads to a drop of the pressure signal, which stagnates at a lower level before increasing again, once the drifter leaves the pool and flows onward in the supraglacial channel.

4 Discussion

4.1 Drifter performance

An investigation of a glacial stream using sensing drifters generally seems to require a significant number of deployments, as the values in Table 4 show, to allow for a statistical analysis and to account for drifter loss and technical problems, which are

https://doi.org/10.5194/tc-2019-132
Preprint. Discussion started: 8 July 2019

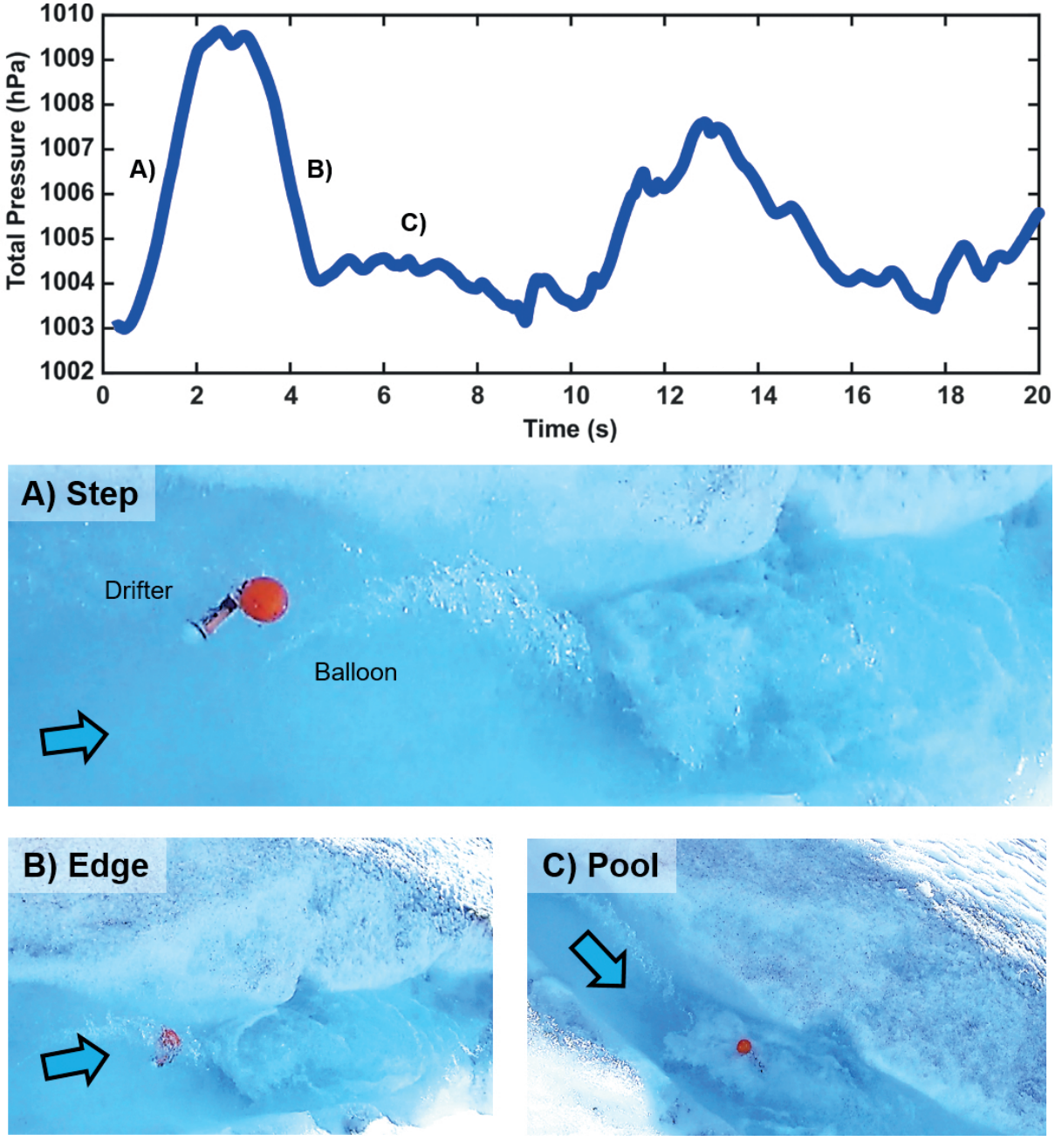

Figure 10. Exemplary data of a drifter going over a step-pool sequence. The plot shows the left pressure record from a single drifter, while passing over a step-pool sequence. The data is averaged over a 2.5 seconds time window. Three zones are marked on the plot, which represent different parts of the passage. A) The total pressure increases, as the drifter travels towards the edge of the step. B) The total pressure drops as the drifter flows over the edge. C) Almost constant pressure values while the drifter is caught in an eddy inside the pool

https://doi.org/10.5194/tc-2019-132
Preprint. Discussion started: 8 July 2019

expressed by the calculation of the utility rate. Pressure values will thereby be the easiest to acquire, as they need the lowest number of deployments compared to the much higher deployment numbers for the IMU values. However, the acquisition of flow data with sensing drifters in glacial channels will require an unrealistic amount of time in the field, and the deployment of many drifters simultaneously to reduce field time and the potential for external factors to influence the measurements (e.g. discharge variations). Bagshaw et al. (2012) previously showed that drifter passage through glacial channels can take several days to weeks, which imposes a practical challenge when it comes to acquiring several hundred to several thousand deployments for statistical analysis. In practice, this is likely to mean that the measurements with sensing drifters will only be possible with higher uncertainty thresholds ($p < 0.05$), as field deployments of several thousand drifters are not realistic. Further technological improvements may significantly decrease the number of necessary deployments, and an updated drifter system will be subject to field testing in summer 2019.

The analysis of the moving means of the signals show that clear features become visible in some of the signals over the channel passage. The analysis of videos from the deployments show that these patterns seem to be related to geometrical features in the flow path such as step-pool sequences and recirculation zones. More data will however be required to verify this hypothesis. Pressure sensors and magnetometer in y-direction seem to produce most clear signal features. The pressure sensors have also the smallest 95% confidence interval of ±0.11% relative to the mean, and deliver the most repeatable data with the lowest error. The confidence intervals for all sensors remain more or less constant over time, some confidence intervals are however larger than others as the sensors travel with different velocities through the channel and pass certain geometric features at different times, which is not accounted for in the plot over time. A part of the higher confidence intervals also comes from the individual drifter movements, such as rotation rate, which are different for every deployment, hence leading to a higher confidence interval. It is however still possible to get pronounced signal features of the IMU readings as well, which can then be linked to geometric features of the channel and flow morphology, as shown in the supplementary video sequences. The IMU readings hereby give an extra value compared to a platform only equipped with pressure sensors, as they can provide the necessary extra information, which will allow us to further distinguish between different geometrical and morphological features of the flow and the channel respectively.

Multi-modal drifters with inertial measurement units present a potentially valuable tool to obtain three-dimensional accelerations along the flow path of a glacial channel. The integration of this data allows to obtain three-dimensional velocity estimates along the channel and to obtain transport surface velocities. This allows for a initial, first order of magnitude estimate of the large-scale (> 10 cm) velocity distribution inside glacier channels, offering a large improvement compared to the state of the art, which relies on point velocities at certain locations through boreholes or integrated velocities along the flow path obtained from dye tracing. The velocities obtained from acceleration integration should however be further constrained with field measurements in future studies to deduce the error introduced by the integration. Nevertheless, the average 95% confidence interval of ±24.5% relative to the mean value clearly implies that further improvements are in order.

https://doi.org/10.5194/tc-2019-132
Preprint. Discussion started: 8 July 2019

It can generally be stated, that the proposed multi-modal drifter platform provides satisfactory overall performance considering the supraglacial field experiments at Foxfonna. The utility rate of 73% in supraglacial channels and 58% of the total deployments in englacial/ subglacial channels provides a first, reasonable estimate of how many sensors a practitioner should consider deploying.

4.2 Glaciological implications

This study establishes that multimodal sensing drifters equipped with pressure sensors and an inertial measurement unit present a new tool to obtain repeatable measurements in supraglacial channels. Further field studies are needed to interpret sensor time series to identify specific features corresponding to channel morphological types and flow conditions. The resulting signal features may be used to provide new insights into the dynamics of glacial hydraulics by overcoming the limitations of existing technologies, which are typically either restricted to a point location or yield only information integrated over the flow path.

We believe that multimodal sensing drifters can also be of great value for the modeling community by providing input for various models, like subglacial hydrology (e.g. Werder et al., 2013) or supraglacial channel development (e.g. Decaux et al., 2019). However, additional fieldwork using ground truth velocities as compared to drifter estimates are necessary. Once this is done, other important studies like linking subglacial hydrology measurements to glacier dynamics can be envisaged. Measurements using sensing drifters can be characterized by comparing them with other widely established measurement techniques, such as those listed in Table 6.

5 Conclusions

The proposed multi-modal drifter platform measures the total water pressure, linear acceleration, magnetic field strength and rotation rate while flowing along a glacial channel. The experiments performed during this study showed that the platform used is able to obtain repeatable data in a 450 m supraglacial stream section. The data are not randomly distributed, but rather show distinct features, which after comparison with video footage of the drifters may be associated with changes in the channel morphology and flow characteristics of the flow. Linking distinct signal variations to channel morphology and flow properties may provide further insights into unknown channel geometries, e.g. in subglacial channels. The multi-modal drifter measurements appear however to require a significant number of repeated deployments to yield repeatable statistics at a 95% confidence interval. This is due to a combination of technical problems and potential deployment losses as well as natural flow variability. The latter will always cause the obtained signals to have variations between different deployments, thus contributing to the estimated significant number of deployments for some of the sensor modalities. Lowering the desired error threshold will however lead to fewer necessary deployments. Pressure measurements seem thereby most feasible for flow path feature detection, as they consistently had low error thresholds and high repeatability. The linear acceleration as measured

https://doi.org/10.5194/tc-2019-132
Preprint. Discussion started: 8 July 2019

Table 6. Potential parameters of interest in subglacial hydrological studies and corresponding available measurement technologies.

Parameter of interest	Dye tracing	Salt dilution gauging	Borehole	Trace gases	GPR	Gauging station	Biogeo-chemistry	Sensing drifters
Discharge	X	X		X		X		
Average velocity	X	X		X		X		X
Channel location			X		X			
Channel geometry	X				X			
Pressure			X			X		X
Temperature			X			X		X
Flow path velocity								X
Water quality						X	X	

by the platform, allowed for an estimation of flow velocities after integration, hence opening up for unprecedented detailed flow dynamic studies. This data may provide novel and rapid ways to investigate the velocity distributions within subglacial channels, after further calibrations of the sensor records to the flow features in glacial channels during follow-up field studies. Those field studies will together with further technological improvements of the proposed platform lead to the availability of a new tool for glacial hydrological studies.

Video supplement. Sample videos of the drifter deployments in supraglacial channels can be found online as video supplements on the journal webpage.

Author contributions. AA, MK and JAT designed and planed the study. AA and MK conducted the fieldwork with support of AJH. AA analysed the data and wrote the manuscript. All authors contributed to the interpretation of the results and the manuscript.

Competing interests. The authors declare that they have no conflict of interest.

https://doi.org/10.5194/tc-2019-132
Preprint. Discussion started: 8 July 2019

Acknowledgements. AA and AK acknowledge partial support by the ERC project ICEMASS. The transport of AA to and from Longyearbyen was provided by Oceanwide Expeditions. Development of the drifter platform and the field costs of MK were paid by the Horizon 2020 FITHydro project as well as the Research Council of Norway through the Centre of Excellence funding scheme, project number 223254 – NTNU AMOS and the Estonian Research Council grants IUT-339 and PUT-1690 Bioinspired Flow Sensing. The University Centre of Svalbard provided logistical support and the TalTECH IT doctoral school provided support for a research stay of AA in Tallinn for data analyses.

https://doi.org/10.5194/tc-2019-132
Preprint. Discussion started: 8 July 2019

References

Almeida, T. G., Walker, D. T., and Warnock, A. M.: Estimating River Bathymetry from Surface Velocity Observations Using Variational Inverse Modeling, Journal of Atmospheric and Oceanic Technology, 35, 21–34, https://doi.org/10.1175/JTECH-D-17-0075.1, 2017.

Anderson, R. S., Anderson, S. P., MacGregor, K. R., Waddington, E. D., O'Neel, S., Riihimaki, C. A., and Loso, M. G.: Strong Feedbacks between Hydrology and Sliding of a Small Alpine Glacier, Journal of Geophysical Research: Earth Surface, 109, 2004.

Bagshaw, E., Lishman, B., Wadham, J., Bowden, J., Burrow, S., Clare, L., and Chandler, D.: Novel Wireless Sensors for in Situ Measurement of Sub-Ice Hydrologic Systems, Annals of Glaciology, 55, 41–50, https://doi.org/10.3189/2014AoG65A007, 2014.

Bagshaw, E. A., Burrow, S., Wadham, J. L., Bowden, J., Lishman, B., Salter, M., Barnes, R., and Nienow, P.: E-Tracers: Development of a Low Cost Wireless Technique for Exploring Sub-Surface Hydrological Systems, Hydrological Processes, 26, 3157–3160, https://doi.org/10.1002/hyp.9451, 2012.

Bagshaw, E. A., Karlsson, N. B., Lok, L. B., Lishman, B., Clare, L., Nicholls, K. W., Burrow, S., Wadham, J. L., Eisen, O., Corr, H., Brennan, P., and Dahl-Jensen, D.: Prototype Wireless Sensors for Monitoring Subsurface Processes in Snow and Firn, Journal of Glaciology, pp. 1–10, https://doi.org/10.1017/jog.2018.76, 2018.

Bartholomew, I., Nienow, P., Sole, A., Mair, D., Cowton, T., and King, M. A.: Short-Term Variability in Greenland Ice Sheet Motion Forced by Time-Varying Meltwater Drainage: Implications for the Relationship between Subglacial Drainage System Behavior and Ice Velocity, Journal of Geophysical Research: Earth Surface, 117, n/a–n/a, https://doi.org/10.1029/2011JF002220, 2012.

Behar, A., Wang, H., Elliot, A., O'Hern, S., Lutz, C., Martin, S., Steffen, K., McGrath, D., and Phillips, T.: The Moulin Explorer: A Novel Instrument to Study Greenland Ice Sheet Melt-Water Flow, IOP Conference Series: Earth and Environmental Science, 6, 012 020, https://doi.org/10.1088/1755-1307/6/1/012020, 2009.

Benn, D., Gulley, J., Luckman, A., Adamek, A., and Glowacki, P. S.: Englacial Drainage Systems Formed by Hydrologically Driven Crevasse Propagation, Journal of Glaciology, 55, 513–523, 2009.

Boydstun, D., Farich, M., III, J. M., Rubinson, S., Smith, Z., and Rekleitis, I.: Drifter Sensor Network for Environmental Monitoring, in: 2015 12th Conference on Computer and Robot Vision, pp. 16–22, https://doi.org/10.1109/CRV.2015.10, 2015.

Cohen, D., Hooyer, T. S., Iverson, N. R., Thomason, J. F., and Jackson, M.: Role of Transient Water Pressure in Quarrying: A Subglacial Experiment Using Acoustic Emissions, Journal of Geophysical Research: Earth Surface, 111, https://doi.org/10.1029/2005JF000439, 2006.

Cohen, J.: A Power Primer, Psychological Bulletin, 112, 155, https://doi.org/10.1037/0033-2909.112.1.155, 1992.

Curran, J. H. and Wohl, E. E.: Large Woody Debris and Flow Resistance in Step-Pool Channels, Cascade Range, Washington, Geomorphology, 51, 141–157, https://doi.org/10.1016/S0169-555X(02)00333-1, 2003.

Decaux, L., Grabiec, M., Ignatiuk, D., and Jania, J.: Role of Discrete Water Recharge from Supraglacial Drainage Systems in Modeling Patterns of Subglacial Conduits in Svalbard Glaciers, The Cryosphere, 13, 735–752, https://doi.org/https://doi.org/10.5194/tc-13-735-2019, 2019.

Diez, A., Matsuoka, K., Jordan, T. A., Kohler, J., Ferraccioli, F., Corr, H. F., Olesen, A. V., Forsberg, R., and Casal, T. G.: Patchy Lakes and Topographic Origin for Fast Flow in the Recovery Glacier System, East Antarctica, Journal of Geophysical Research: Earth Surface, 124, 287–304, https://doi.org/10.1029/2018JF004799, 2019.

Engelhardt, H. and Kamb, B.: Basal Sliding of Ice Stream B, West Antarctica, Journal of Glaciology, 44, 223–230, https://doi.org/10.3189/S0022143000002562, 1998.

https://doi.org/10.5194/tc-2019-132
Preprint. Discussion started: 8 July 2019

Engelhardt, H., Humphrey, N., Kamb, B., and Fahnestock, M.: Physical Conditions at the Base of a Fast Moving Antarctic Ice Stream, Science, 248, 57–59, https://doi.org/10.1126/science.248.4951.57, 1990.

Flowers, G. E.: Hydrology and the Future of the Greenland Ice Sheet, Nature Communications, 9, 2729, https://doi.org/10.1038/s41467-018-05002-0, 2018.

Fountain, A. G.: Geometry and Flow Conditions of Subglacial Water at South Cascade Glacier, Washington State, U.S.A.; an Analysis of Tracer Injections, Journal of Glaciology, 39, 143–156, https://doi.org/10.3189/S0022143000015793, 1993.

Germain, S. L. S. and Moorman, B. J.: The Development of a Pulsating Supraglacial Stream, Annals of Glaciology, 57, 31–38, https://doi.org/10.1017/aog.2016.16, 2016.

Goodman, D. J., King, G. C. P., Millar, D. H. M., and Robin, G. d. Q.: Pressure-Melting Effects in Basal Ice of Temperate Glaciers: Laboratory Studies and Field Observations Under Glacier D'Argentière, Journal of Glaciology, 23, 259–271, https://doi.org/10.1017/S0022143000029889, 1979.

Gulley, J., Benn, D., Müller, D., and Luckman, A.: A Cut-and-Closure Origin for Englacial Conduits in Uncrevassed Regions of Polythermal Glaciers, Journal of Glaciology, 55, 66–80, https://doi.org/10.3189/002214309788608930, 2009.

Haldorsen, S.: Grain-Size Distribution of Subglacial till and Its Realtion to Glacial Scrushing and Abrasion, Boreas, 10, 91–105, https://doi.org/10.1111/j.1502-3885.1981.tb00472.x, 1981.

Hantz, D. and Lliboutry, L.: Waterways, Ice Permeability at Depth, and Water Pressures at Glacier D'Argentière, French Alps, Journal of Glaciology, 29, 227–239, https://doi.org/10.3189/S0022143000008285, 1983.

Harper, J. T., Bradford, J. H., Humphrey, N. F., and Meierbachtol, T. W.: Vertical Extension of the Subglacial Drainage System into Basal Crevasses, Nature, 467, 579, 2010.

Hart, J. K., Martinez, K., Ong, R., Riddoch, A., Rose, K. C., and Padhy, P.: A Wireless Multi-Sensor Subglacial Probe: Design and Preliminary Results, Journal of Glaciology, 52, 389–397, https://doi.org/10.3189/172756506781828575, 2006.

Hart, J. K., Rose, K. C., and Martinez, K.: Subglacial till Behaviour Derived from in Situ Wireless Multi-Sensor Subglacial Probes: Rheology, Hydro-Mechanical Interactions and till Formation, Quaternary Science Reviews, 30, 234–247, https://doi.org/10.1016/j.quascirev.2010.11.001, 2011a.

Hart, J. K., Rose, K. C., Waller, R. I., Vaughan-Hirsch, D., and Martinez, K.: Assessing the Catastrophic Break-up of Briksdalsbreen, Norway, Associated with Rapid Climate Change, Journal of the Geological Society, 168, 673–688, https://doi.org/10.1144/0016-76492010-024, 2011b.

Hart, J. K., Rose, K. C., Clayton, A., and Martinez, K.: Englacial and Subglacial Water Flow at Skálafellsjökull, Iceland Derived from Ground Penetrating Radar, in Situ Glacsweb Probe and Borehole Water Level Measurements, Earth Surface Processes and Landforms, 40, 2071–2083, https://doi.org/10.1002/esp.3783, 2015.

Hart, J. K., Martinez, K., Basford, P. J., Clayton, A. I., Robson, B. A., and Young, D. S.: Surface Melt Driven Summer Diurnal and Winter Multi-Day Stick-Slip Motion and till Sedimentology, Nature Communications, 10, 1599, https://doi.org/10.1038/s41467-019-09547-6, 2019.

Hasnain, S. I., Jose, P. G., Ahmad, S., and Negi, D. C.: Character of the Subglacial Drainage System in the Ablation Area of Dokriani Glacier, India, as Revealed by Dye-Tracer Studies, Journal of Hydrology, 248, 216–223, https://doi.org/10.1016/S0022-1694(01)00404-8, 2001.

Hou, H., Deng, Z., Martinez, J., Fu, T., Duncan, J., Johnson, G., Lu, J., Skalski, J., Townsend, R., and Tan, L.: A Hydropower Biological Evaluation Toolset (HBET) for Characterizing Hydraulic Conditions and Impacts of Hydro-Structures on Fish, Energies, 11, 990, 2018.

https://doi.org/10.5194/tc-2019-132
Preprint. Discussion started: 8 July 2019

How, P., Benn, D. I., Hulton, N. R. J., Hubbard, B., Luckman, A., Sevestre, H., van Pelt, W. J. J., Lindbäck, K., Kohler, J., and Boot, W.: Rapidly Changing Subglacial Hydrological Pathways at a Tidewater Glacier Revealed through Simultaneous Observations of Water Pressure, Supraglacial Lakes, Meltwater Plumes and Surface Velocities, The Cryosphere, 11, 2691–2710, https://doi.org/10.5194/tc-11-2691-2017, 2017.

Hubbard, B. and Nienow, P.: Alpine Subglacial Hydrology, Quaternary Science Reviews, 16, 939–955, 1997.

Hubbard, B. P., Sharp, M. J., Willis, I. C., Nielsen, M. K., and Smart, C. C.: Borehole Water-Level Variations and the Structure of the Subglacial Hydrological System of Haut Glacier d'Arolla, Valais, Switzerland, Journal of Glaciology, 41, 572–583, https://doi.org/10.3189/S0022143000034894, 1995.

Iken, A.: Measurements of Water Pressure in Moulins as Part of a Movement Study of the White Glacier, Axel Heiberg Island, Northwest Territories, Canada, Journal of Glaciology, 11, 53–58, https://doi.org/10.3189/S0022143000022486, 1972.

Iken, A. and Bindschadler, R. A.: Combined Measurements of Subglacial Water Pressure and Surface Velocity of Findelengletscher, Switzerland: Conclusions about Drainage System and Sliding Mechanism, Journal of Glaciology, 32, 101–119, https://doi.org/10.3189/S0022143000006936, 1986.

Isenko, E., Naruse, R., and Mavlyudov, B.: Water Temperature in Englacial and Supraglacial Channels: Change along the Flow and Contribution to Ice Melting on the Channel Wall, Cold Regions Science and Technology, 42, 53–62, https://doi.org/10.1016/j.coldregions.2004.12.003, 2005.

Iverson, N. R., Hooyer, T. S., Fischer, U. H., Cohen, D., Moore, P. L., Jackson, M., Lappegard, G., and Kohler, J.: Soft-Bed Experiments beneath Engabreen, Norway: Regelation Infiltration, Basal Slip and Bed Deformation, Journal of Glaciology, 53, 323–340, https://doi.org/10.3189/002214307783258431, 2007.

Jaffe, J. S., Franks, P. J. S., Roberts, P. L. D., Mirza, D., Schurgers, C., Kastner, R., and Boch, A.: A Swarm of Autonomous Miniature Underwater Robot Drifters for Exploring Submesoscale Ocean Dynamics, Nature Communications, 8, 14 189, https://doi.org/10.1038/ncomms14189, 2017.

Jarosch, A. H. and Gudmundsson, M. T.: A Numerical Model for Meltwater Channel Evolution in Glaciers, The Cryosphere, 6, 493–503, https://doi.org/10.5194/tc-6-493-2012, 2012.

Kor, P. S. G., Shaw, J., and Sharpe, D. R.: Erosion of Bedrock by Subglacial Meltwater, Georgian Bay, Ontario: A Regional View, Canadian Journal of Earth Sciences, 28, 623–642, https://doi.org/10.1139/e91-054, 1991.

Kullback, S. and Leibler, R. A.: On Information and Sufficiency, The Annals of Mathematical Statistics, 22, 79–86, https://doi.org/10.1214/aoms/1177729694, 1951.

Landon, K. C., Wilson, G. W., Özkan-Haller, H. T., and MacMahan, J. H.: Bathymetry Estimation Using Drifter-Based Velocity Measurements on the Kootenai River, Idaho, Journal of Atmospheric and Oceanic Technology, 31, 503–514, https://doi.org/10.1175/JTECH-D-13-00123.1, 2014.

Lishman, B., Wadham, J., Drinkwater, B., Kendall, J.-M., Burrow, S., Hilton, G., and Craddock, I.: Assessing the Utility of Acoustic Communication for Wireless Sensors Deployed beneath Ice Sheets, Annals of Glaciology, 54, 124–134, https://doi.org/10.3189/2013AoG64A022, 2013.

Lock, G. S. H.: The Growth and Decay of Ice, Cambridge University Press, 1990.

Martinez, K., Hart, J. K., and Ong, R.: Environmental Sensor Networks, Computer, 37, 50–56, https://doi.org/10.1109/MC.2004.91, 2004.

Martinez, K., Hart, J. K., Basford, P. J., Bragg, G. M., Ward, T., and Young, D. S.: A Geophone Wireless Sensor Network for Investigating Glacier Stick-Slip Motion, Computers & Geosciences, 105, 103–112, https://doi.org/10.1016/j.cageo.2017.05.005, 2017.

Meire, L., Mortensen, J., Meire, P., Juul-Pedersen, T., Sejr, M. K., Rysgaard, S., Nygaard, R., Huybrechts, P., and Meysman, F. J. R.: Marine-Terminating Glaciers Sustain High Productivity in Greenland Fjords, Global Change Biology, 23, 5344–5357, https://doi.org/10.1111/gcb.13801, 2017.

Nienow, P., Sharp, M., and Willis, I.: Seasonal Changes in the Morphology of the Subglacial Drainage System, Haut Glacier d'Arolla, Switzerland, Earth Surface Processes and Landforms, 23, 825–843, https://doi.org/10.1002/(SICI)1096-9837(199809)23:9<825::AID-ESP893>3.0.CO;2-2, 1998.

Rada, C. and Schoof, C.: Channelized, Distributed, and Disconnected: Subglacial Drainage under a Valley Glacier in the Yukon, The Cryosphere, 12, 2609–2636, https://doi.org/10.5194/tc-12-2609-2018, 2018.

Rose, K. C., Hart, J. K., and Martinez, K.: Seasonal Changes in Basal Conditions at Briksdalsbreen, Norway: The Winter–Spring Transition, Boreas, 38, 579–590, https://doi.org/10.1111/j.1502-3885.2008.00079.x, 2009.

Röthlisberger, H.: Water Pressure in Intra- and Subglacial Channels, Journal of Glaciology, 11, 177–203, https://doi.org/10.3189/S0022143000022188, 1972.

Schoof, C.: Ice-Sheet Acceleration Driven by Melt Supply Variability, Nature, 468, 803, https://doi.org/10.1038/nature09618, 2010.

Schuler, T. V. and Fischer, U. H.: Modeling the Diurnal Variation of Tracer Transit Velocity through a Subglacial Channel, Journal of Geophysical Research, 114, https://doi.org/10.1029/2008JF001238, 2009.

Seaberg, S. Z., Seaberg, J. Z., Hooke, R. L., and Wiberg, D. W.: Character of the Englacial and Subglacial Drainage System in the Lower Part of the Ablation Area of Storglaciären, Sweden, as Revealed by Dye-Trace Studies, Journal of Glaciology, 34, 217–227, https://doi.org/10.3189/S0022143000032263, 1988.

Smeets, C. J. P. P., Boot, W., Hubbard, A., Pettersson, R., Wilhelms, F., Broeke, M. R. V. D., and Wal, R. S. W. V. D.: A Wireless Subglacial Probe for Deep Ice Applications, Journal of Glaciology, 58, 841–848, https://doi.org/10.3189/2012JoG11J130, 2012.

Stearns, L. A. and van der Veen, C. J.: Friction at the Bed Does Not Control Fast Glacier Flow, Science, 361, 273–277, https://doi.org/10.1126/science.aat2217, 2018.

Stone, D. B. and Clarke, G. K. C.: In Situ Measurements of Basal Water Quality and Pressure as an Indicator of the Character of Subglacial Drainage Systems, Hydrological Processes, 10, 615–628, https://doi.org/10.1002/(SICI)1099-1085(199604)10:4<615::AID-HYP395>3.0.CO;2-M, 1996.

Sundal, A. V., Shepherd, A., Nienow, P., Hanna, E., Palmer, S., and Huybrechts, P.: Melt-Induced Speed-up of Greenland Ice Sheet Offset by Efficient Subglacial Drainage, Nature, 469, 521, 2011.

Swift, D. A., Nienow, P. W., and Hoey, T. B.: Basal Sediment Evacuation by Subglacial Meltwater: Suspended Sediment Transport from Haut Glacier d'Arolla, Switzerland, Earth Surface Processes and Landforms, 30, 867–883, https://doi.org/10.1002/esp.1197, 2005.

Urbanski, J. A., Stempniewicz, L., Węsławski, J. M., Dragańska-Deja, K., Wochna, A., Goc, M., and Iliszko, L.: Subglacial Discharges Create Fluctuating Foraging *Hotspots* for Sea Birds in Tidewater Glacier Bays, Scientific Reports, 7, 43 999, https://doi.org/10.1038/srep43999, 2017.

Van de Wal, R. S. W., Boot, W., Van den Broeke, M. R., Smeets, C., Reijmer, C. H., Donker, J. J. A., and Oerlemans, J.: Large and Rapid Melt-Induced Velocity Changes in the Ablation Zone of the Greenland Ice Sheet, science, 321, 111–113, 2008.

van de Wal, R. S. W., Smeets, C. J. P. P., Boot, W., Stoffelen, M., van Kampen, R., Doyle, S. H., Wilhelms, F., van den Broeke, M. R., Reijmer, C. H., Oerlemans, J., and Hubbard, A.: Self-Regulation of Ice Flow Varies across the Ablation Area in South-West Greenland, The Cryosphere, 9, 603–611, https://doi.org/https://doi.org/10.5194/tc-9-603-2015, 2015.

https://doi.org/10.5194/tc-2019-132
Preprint. Discussion started: 8 July 2019

Vatne, G. and Irvine-Fynn, T. D. L.: Morphological Dynamics of an Englacial Channel, Hydrology and Earth System Sciences, 20, 2947–2964, https://doi.org/https://doi.org/10.5194/hess-20-2947-2016, 2016.

Vieli, A., Jania, J., Blatter, H., and Funk, M.: Short-Term Velocity Variations on Hansbreen, a Tidewater Glacier in Spitsbergen, Journal of Glaciology, 50, 389–398, https://doi.org/10.3189/172756504781829963, 2004.

Vivian, R. and Bocquet, G.: Subglacial Cavitation Phenomena Under the Glacier D'Argentière, Mont Blanc, France, Journal of Glaciology, 12, 439–451, https://doi.org/10.3189/S0022143000031853, 1973.

Walder, J. S. and Fowler, A.: Channelized Subglacial Drainage over a Deformable Bed, Journal of Glaciology, 40, 3–15, 1994.

Weertman, J.: General Theory of Water Flow at the Base of a Glacier or Ice Sheet, Reviews of Geophysics, 10, 287–333, https://doi.org/10.1029/RG010i001p00287, 1972.

Werder, M. A., Hewitt, I. J., Schoof, C. G., and Flowers, G. E.: Modeling Channelized and Distributed Subglacial Drainage in Two Dimensions, Journal of Geophysical Research: Earth Surface, 118, 2140–2158, https://doi.org/10.1002/jgrf.20146, 2013.

Willis, I. C., Sharp, M. J., and Richards, K. S.: Configuration of the Drainage System of Midtdalsbreen, Norway, as Indicated by Dye-Tracing Experiments, Journal of Glaciology, 36, 89–101, https://doi.org/10.3189/S0022143000005608, 1990.

Willis, I. C., Fitzsimmons, C. D., Melvold, K., Andreassen, L. M., and Giesen, R. H.: Structure, Morphology and Water Flux of a Subglacial Drainage System, Midtdalsbreen, Norway, Hydrological Processes, 26, 3810–3829, https://doi.org/10.1002/hyp.8431, 2012.

Zwally, H. J., Abdalati, W., Herring, T., Larson, K., Saba, J., and Steffen, K.: Surface Melt-Induced Acceleration of Greenland Ice-Sheet Flow, Science, 297, 218–222, 2002.